Electronic Supplementary Information (ESI)

The electrochemical corrosion of air thermal-treated carbon fiber cloth electrocatalyst with outstanding oxygen evolution activity under alkaline condition

Tianxing Wu,[†] Miaomiao Han,[†] Xiaoguang Zhu,[†] Guozhong Wang,[†] Haimin Zhang[†,*] and Huijun Zhao[†,§]

[†] Key Laboratory of Materials Physics, Centre for Environmental and Energy Nanomaterials, Anhui Key Laboratory of Nanomaterials and Nanotechnology, CAS Center for Excellence in Nanoscience, Institute of Solid State Physics, Chinese Academy of Sciences, Hefei, 230031 Anhui, PR China

[§] Centre for Clean Environment and Energy, Griffith University, Gold Coast Campus, QLD 4222, Australia

*E-mail: zhanghm@issp.ac.cn (Haimin Zhang)

Experimental section

Materials： Carbon fiber cloth (CFC) was purchased from Shanghai Hesen Electric Co., Ltd. Potassium hydroxide (KOH) was purchased from Aladdin Ltd. (Shanghai, China). Anhydrous ethanol was purchased from Sinopharm Chemical Reagent Co., Ltd. (Shanghai, China). Commercial RuO_2 powder (99.9%) was purchased from Sigma-Aldrich. All the chemicals were used as received without further purification.

Thermal-treated CFC in air： Commercial CFC, which was washed with deionized water and anhydrous ethanol for three times, then dried in air and cut into 1.0×2.0 cm for use. The cleaned CFC was annealed in a box-type furnace at different temperature (400, 450, 500 and 550 ^{o}C) for 2 h in air atmosphere at a heating rate of 5 ^{o}C min^{-1}. The obtained products were denoted as CFC-X (X=400, 450, 500 and 550, respectively).

Characterizations： Morphological properties of the samples were investigated by a field emission scanning electron microscopy (FESEM, SU8020) operated at an accelerating voltage of 10.0 kV. The microstructure of samples was examined by a high resolution transmission electron microscopy (HRTEM, Tecnai G2 F20) with an acceleration voltage of 200 kV. The thermal stability of the samples was assessed using a thermogravimetric analyzer (Pyris 1 TGA, Perkin-Elmer), where the samples were heated at 5 ^{o}C min^{-1} from 50 to 700 ^{o}C. Raman spectra were carried out on a LabRAM HR800 confocal microscope Raman system (Horiba Jobin Yvon) using an Ar ion laser operating at 532 nm. XPS analysis of the samples was performed on an ESCALAB 250 X-ray photoelectron spectrometer (Thermo, America) equipped with Al $K\alpha_{1,2}$ monochromatized radiation at 1486.6 eV X-ray source. PL spectra were recorded by a

F7000 Fluorescence Spectrophotometer (Hitachi, Japan) with slit width of 0.5 mm. The surface area and porosity of samples were measured by a Surface Area and Porosity Analyzer (Tristar 3020M).

Electrochemical measurements： The electrochemical measurements of OER performance were performed in a standard three-electrode system in 20 mL 1.0 M KOH (pH=14) controlled by a CHI 760E electrochemical workstation (CH Instruments, Inc., Shanghai, China). The as-obtained CFC samples (1.0×2.0 cm) were directly used as the working electrode, and the effective geometric area was 1.0×1.0 cm^2. A piece of cleaned CFC (1.5×2.0 cm) was used as counter electrode. Hg/HgO electrode was used as reference electrode in KOH electrolyte, respectively. Linear sweep voltammetry (LSV) curves without *iR* compensation were conducted in 1.0 M KOH electrolyte with a scan rate of 1.0 mV s^{-1}. All the potentials reported in this work were calibrated to a reversible hydrogen electrode (RHE), which was expressed as (E (*vs*. RHE) = E (*vs*. Hg/HgO) + 0.925 V). For the purpose of comparison, the OER performance of the commercial RuO_2 (99.9%, Sigma-Aldrich) was also measured under the identical experimental conditions similar with the measurement conditions using CFC electrodes. RuO_2 ink was prepared by dispersing 5.0 mg commercial RuO_2 in 500 μL of mixed solution containing 400 μL of deionized water, 95 μL of ethanol and 5 μL of 5 wt.% Nafion solution. After ultrasonic dispersion, the RuO_2 ink was loaded onto CFC substrate (1.0×1.0 cm) and then dried at room temperature. The obtained sample was denoted as RuO_2/CFC.

Computational methods： All the first-principle calculations were performed within

the framework of density functional theory (DFT) as implemented in the Vienna ab-initio Simulation Package (VASP). The projector augmented wave (PAW) method has been used to describe the inert core electrons with the C-$2s^2 2p^2$, O-$2s^2 2p^4$, H-$1s^1$ treated as the valence electrons. A cut off energy of 450 eV was used for the expansion of the wave functions. The electronic exchange-correlation effects were described with Perdew-Burke-Ernzerhof generalized gradient approximation (PBE-GGA) functional.

There are two kinds of graphene nanoribbons with zigzag edge or armchair edge. Armchair nanoribbon can be semiconducting or metallic depending on width, while zigzag nanoribbon is always metallic and of greater stability, which possesses great advantages on electrochemical catalysis reaction.[1] Taking these into consideration, zigzag nanoribbon was chosen as the basic model. The zigzag graphene nanoribbon (GNR) was modeled as three-dimensional periodic structures, where vacuum layers were set around 14 Å and 18 Å in the x- and z-directions, respectively. The gamma (Γ) centered 1×1×1 Monkhorst-Pack k-point sampling was used. The Fermi level was slightly broadened using a Fermi-Dirac smearing of 50 meV. All calculations were spin polarized and full relaxations were done until the force of the system converges to 0.05 eV $Å^{-1}$.

The oxygen evolution reaction (OER) was considered via the four-step four-electron reaction paths for zigzag GNR with different C=O contents. In alkaline environment, OER can be written as:[2]

$$OH^- + * \rightarrow OH^* + e^- \quad (1)$$

$$OH^* + OH^- \rightarrow O^* + H_2O\ (l) + e^- \quad (2)$$

$$O^* + OH^- \rightarrow OOH^* + e^- \quad (3)$$

$$OOH^* + OH^- \rightarrow * + O_2\,(g) + H_2O\,(l) + e^- \quad (4)$$

where * stands for an active site on the graphene surface, (l) and (g) refer to liquid and gas phases, respectively, and OH*, O* and OOH* are adsorbed intermediates.

The overpotential of OER process was determined by examining the reaction free-energies of the different elementary steps. For each step, the reaction free energy ΔG is defined as the difference between free energies of the initial and final states and is given by the following expression:

$$\Delta G = \Delta E + \Delta ZPE - T\Delta S + \Delta G_U + \Delta G_{pH} \quad (5)$$

where ΔE is the reaction energy of reactant and product molecules adsorbed on catalyst surface obtained from DFT calculations, ΔZPE is the change of zero-point energy, T is the temperature and ΔS is the entropy change. For the adsorbed species, only the vibrational frequencies and entropy were considered for the energy correction.

$\Delta G_U = -eU$, where e is the charge transferred and U is the potential at the electrode. ΔG_{pH} is free energy correction of the H^+ by the concentration dependence of the entropy:

$$\Delta G_{pH} = -k_B T \ln[H^+] \quad (6)$$

For OER, the overpotential can be obtained from:

$$G^{OER} = \max\{\Delta G_1, \Delta G_2, \Delta G_3, \Delta G_4\} \quad (7)$$

$$\eta^{OER} = G^{OER}/e - 1.23\ V \quad (8)$$

where ΔG_1, ΔG_2, ΔG_3, ΔG_4 are the reaction free energy of (1)-(4), respectively.

Table S1. Comparison of selected state-of-the-art metal-free electrocatalysts in the oxygen evolution reaction.

Catalysts	Electrolytes	Substrate	Overpotential (mV) for OER at specific current density	Reference
CFC-450	1.0 M KOH	free-standing	224 @ 10 mA cm^{-2}	This work
PEMAc@CNTs90	1.0 M KOH	GCE	298 @ 10 mA cm^{-2}	[3]
Echo-MWCNTs	1.0 M KOH	GCE	360 @ 10 mA cm^{-2}	[4]
ONPPGC/OCC	1.0 M KOH	carbon cloth	410 @ 10 mA cm^{-2}	[5]
N-doped porous CC	1.0 M KOH	carbon cloth	360 @ 10 mA cm^{-2}	[6]
Defective graphene	1.0 M KOH	GCE	340 @ 10 mA cm^{-2}	[7]
P-doped graphene	1.0 M KOH	GCE	330 @ 10 mA cm^{-2}	[8]
Surface-oxidized carbon black	1.0 M KOH	GCE	440 @ 10 mA cm^{-2}	[9]
P-CC	1.0 M KOH	free-standing	450 @ 10 mA cm^{-2}	[2]
N/C	0.1 M KOH	GCE	380 @ 10 mA cm^{-2}	[10]
G-CNT	0.1 M KOH	GCE	498 @ 5 mA cm^{-2}	[11]
NG-CNT	0.1 M KOH	GCE	368 @ 5 mA cm^{-2}	
g-C_3N_4	0.1 M KOH	GCE	734 @ 10 mA cm^{-2}	[12]

g-C_3N_4/graphene	0.1 M KOH	GCE	539 @ 10 mA cm^{-2}	
g-C_3N_4/NS-CNT	0.1 M KOH	GCE	370 @ 10 mA cm^{-2}	[13]
Oxidized carbon cloth	0.1 M KOH	GCE	477 @ 10 mA cm^{-2}	[14]
NCNF-1000	0.1 M KOH	GCE	610 @ 10 mA cm^{-2}	[15]
NGM	0.1 M KOH	GCE	440 @ 10 mA cm^{-2}	[16]
Black phosphorous	0.1 M KOH	Ti	370 @ 10 mA cm^{-2}	[17]
BP-CNT		GCE	320 @ 10 mA cm^{-2}	

Table S2. The percent composition for C=O, C-OH, C-OOH and H-O-H in the samples of pristine CFC, CFC-400 and CFC-450 as obtained by XPS.

Samples	O 1s (at.%)	C=O (at.%)	C-OH (at.%)	C-OOH (at.%)	H-O-H (at.%)
CFC	4.96	1.36	1.30	1.66	0.64
CFC-400	2.67	1.34	0.88	0.42	0.03
CFC-450	2.55	0.68	0.55	0.85	0.47

Table S3. Nitrogen sorption-derived textural properties of CFC and CFC-450 after long term chronoamperometric measurement under 1.375 V for 1 h, respectively.

Sample	BET Surface Area ($m^2\ g^{-1}$)	Pore Volume ($cm^3\ g^{-1}$)	Pore Size (nm)
CFC-450	13.45	0.018	1.97
CFC-450 after OER	556.20	17.83	44.86

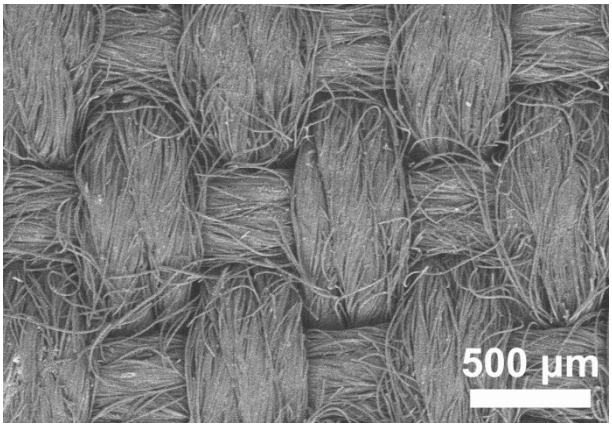

Fig. S1 Low-magnification SEM image of pristine CFC.

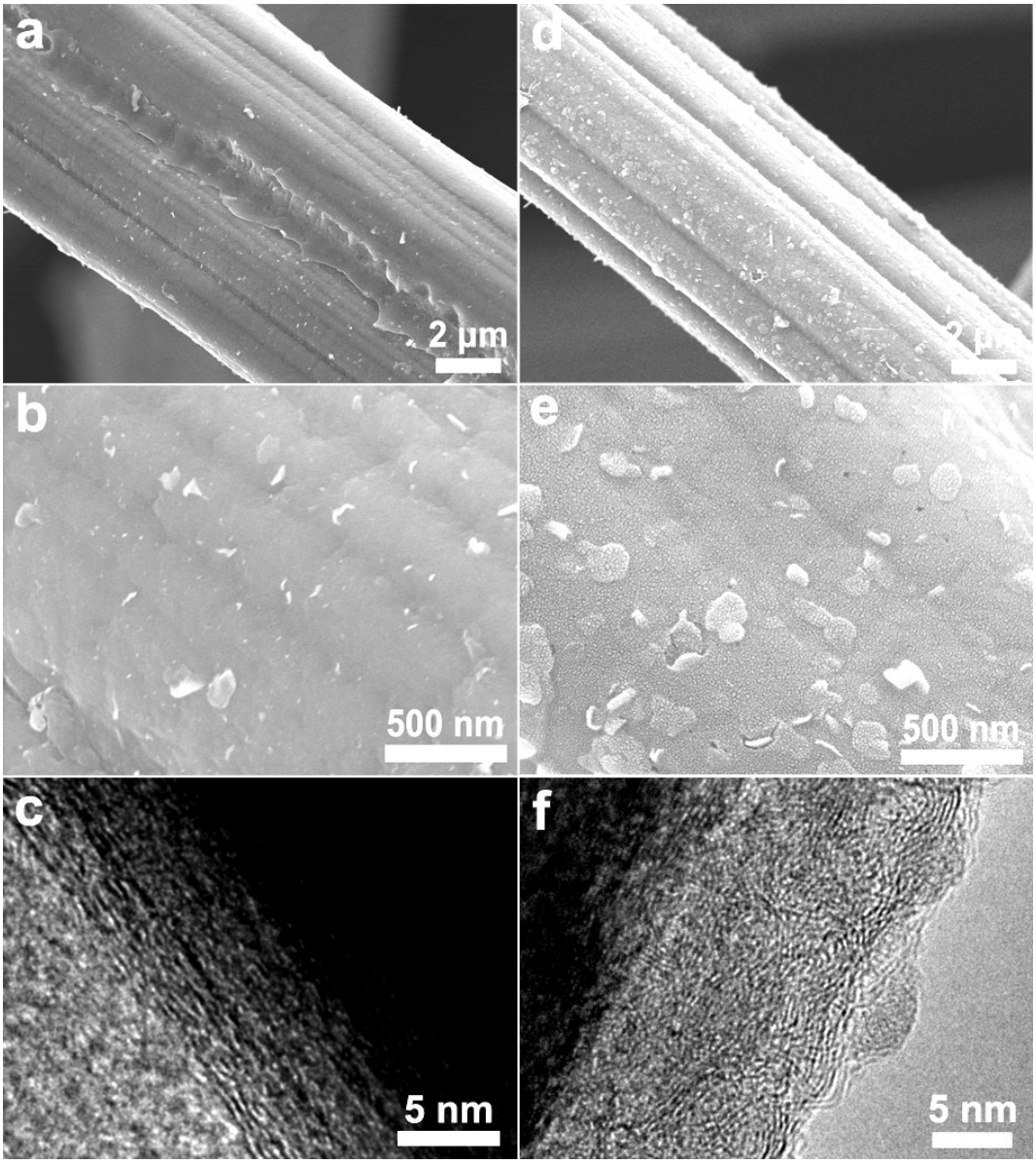

Fig. S2 SEM and HRTEM images of CFC (a-c) and CFC-450 (d-f).

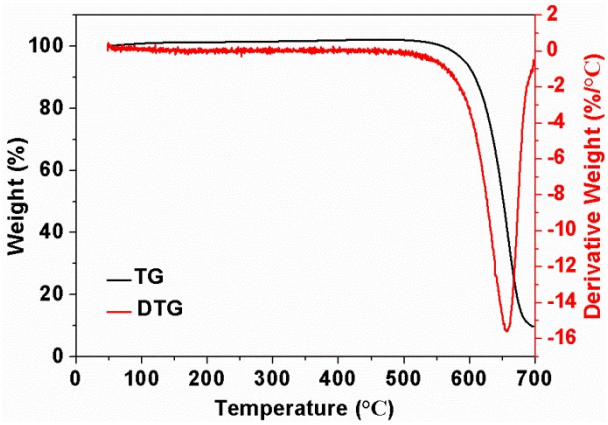

Fig. S3 TGA curves of pristine CFC.

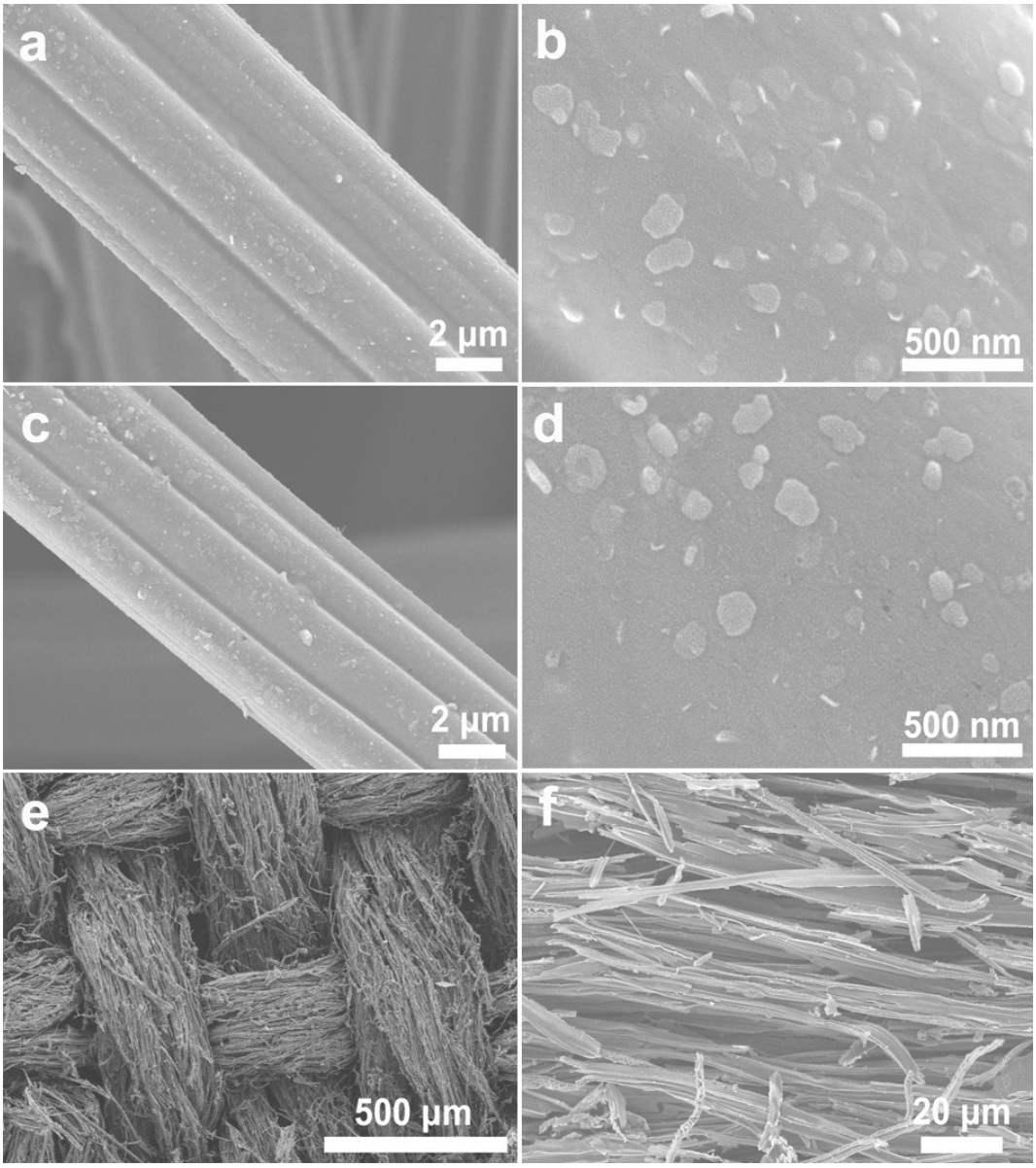

Fig. S4 SEM images of (a-b) CFC-400, (c-d) CFC-500 and (e-f) CFC-550.

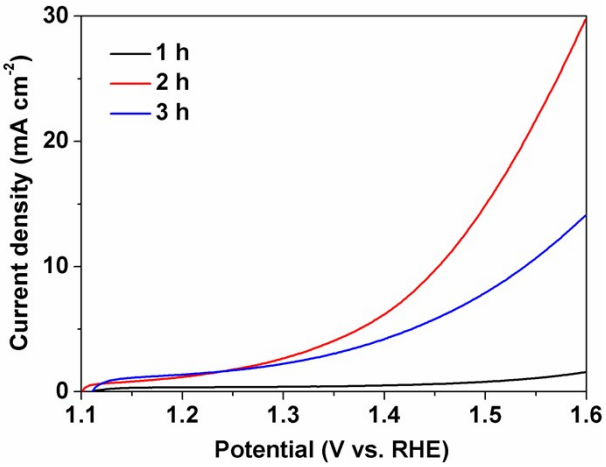

Fig. S5 Polarization curves of CFC after annealed at 450 °C for different time (1 h, 2 h and 3 h) with a scan rate of 1.0 mV s^{-1} in 1.0 M KOH electrolyte.

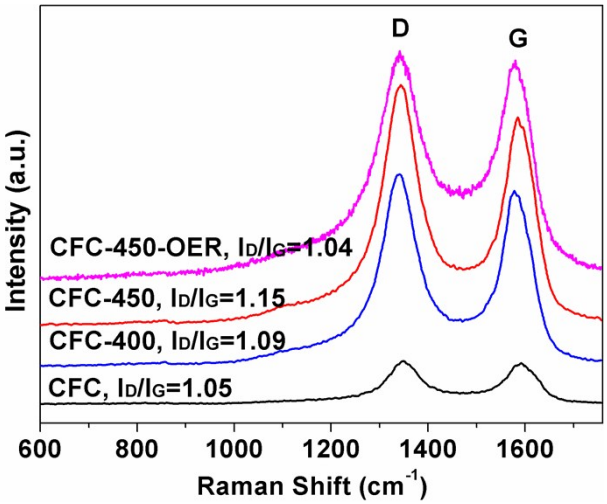

Fig. S6 Raman spectra of CFC, CFC-400, CFC-450 and CFC-450 after LSV scanning in 1.0 M KOH electrolyte.

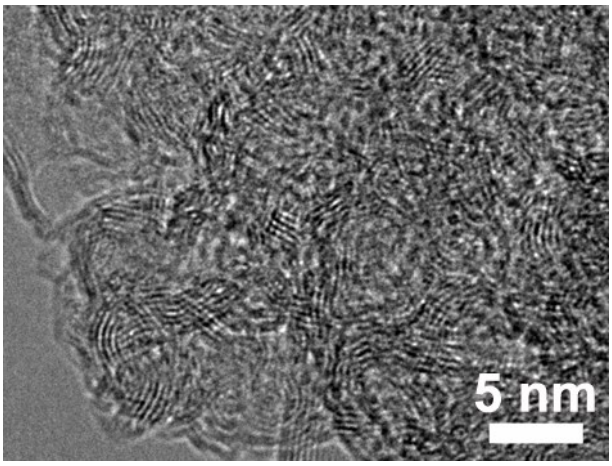

Fig. S7 High resolution TEM image of CFC-450 after LSV scanning in 1.0 M KOH electrolyte.

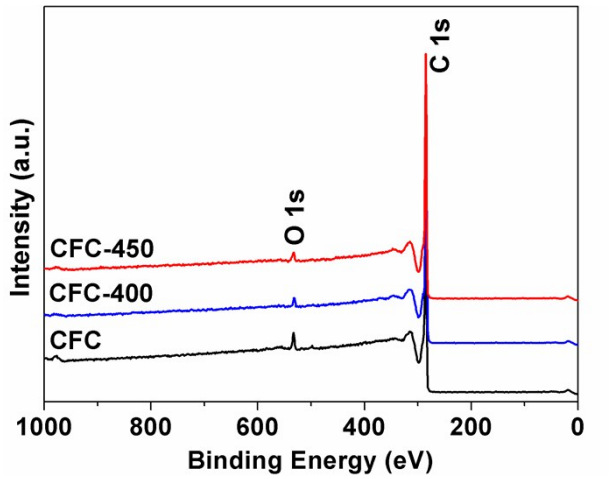

Fig. S8 XPS survey spectra of pristine CFC, CFC-400 and CFC-450.

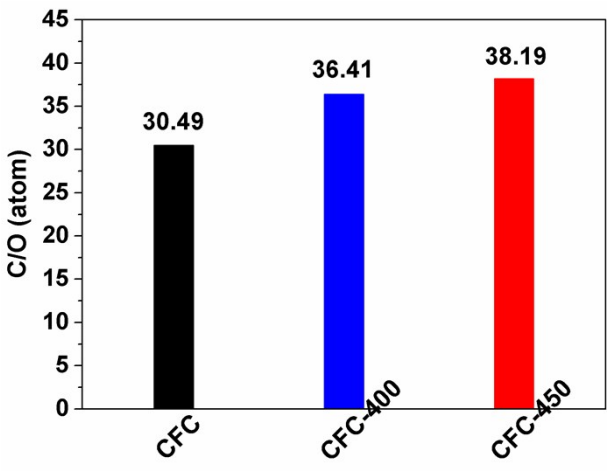

Fig. S9 The values of C/O (atom) for pristine CFC, CFC-400 and CFC-450 as obtained by XPS.

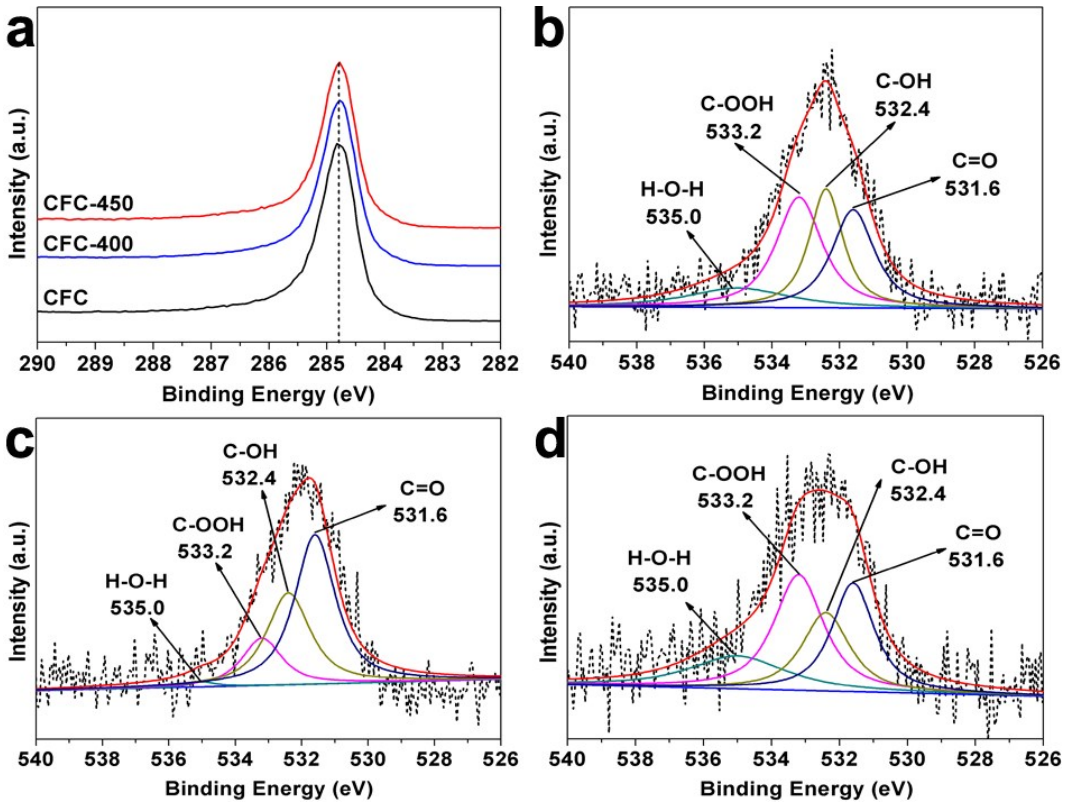

Fig. S10 (a) High resolution C 1s XPS spectra of pristine CFC, CFC-400 and CFC-450. High resolution O 1s XPS spectra of: (b) pristine CFC, (c) CFC-400 and (d) CFC-450.

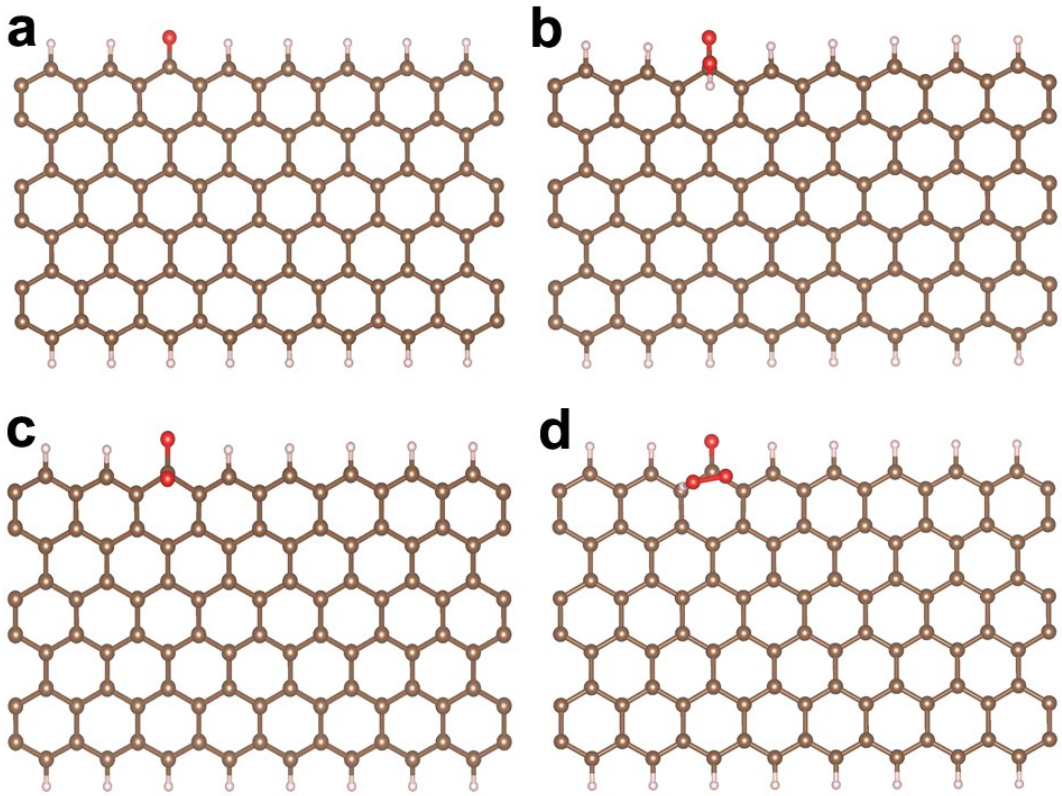

Fig. S11 Schematic representations of the OER pathways on the zigzag graphene nanoribbon with one C=O group: (a) C=O graphene before OER; (b) adsorption of OH; (c) adsorption of O; (d) adsorption of OOH.

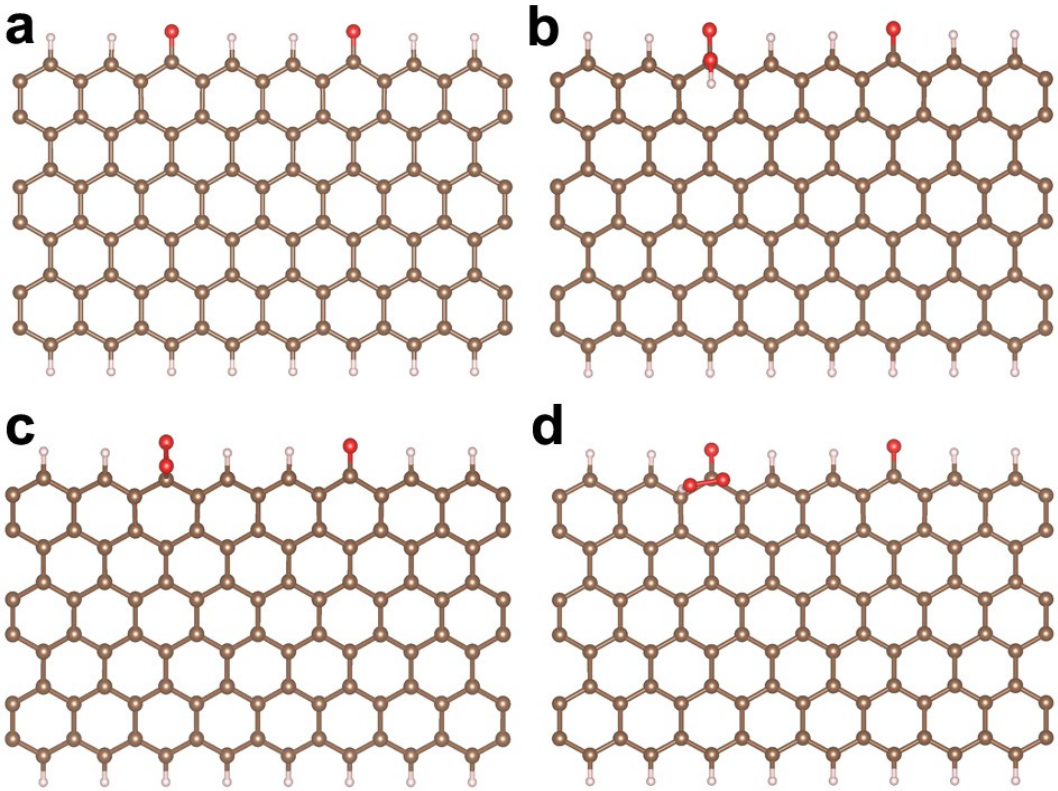

Fig. S12 Schematic representations of the OER pathways on the zigzag graphene nanoribbon with two C=O groups: (a) C=O graphene before OER; (b) adsorption of OH; (c) adsorption of O; (d) adsorption of OOH.

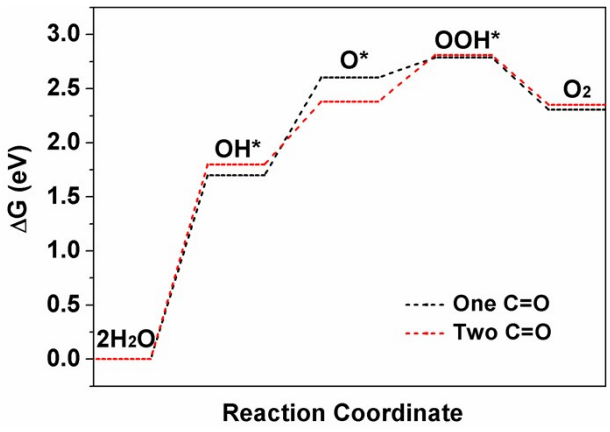

Fig. S13 Free energy diagrams of OER at U=0 V for the zigzag graphene nanoribbon with one or two C=O in 1.0 M KOH electrolyte.

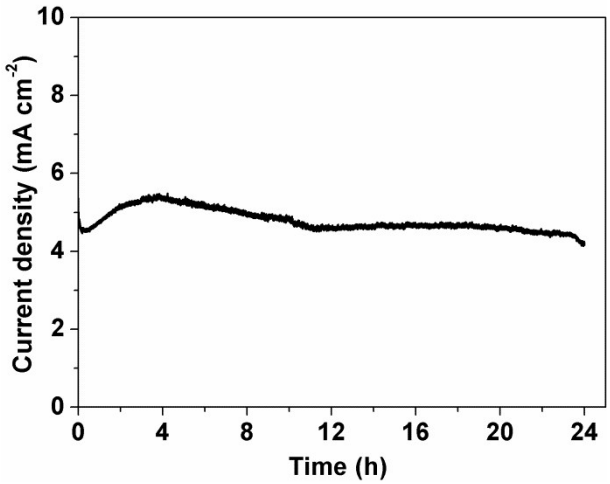

Fig. S14 Time-dependent current density curve for CFC-450 under static potential (1.375 V vs. RHE) for 24 h in 1.0 M KOH electrolyte.

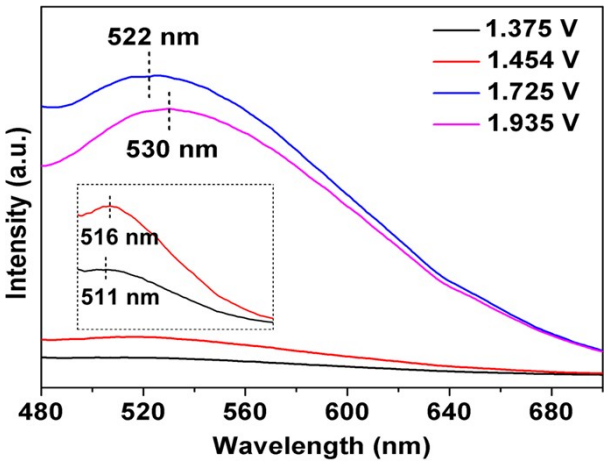

Fig. S15 PL spectra of solutions obtained under different static potentials with excitation wavelength of 365 nm.

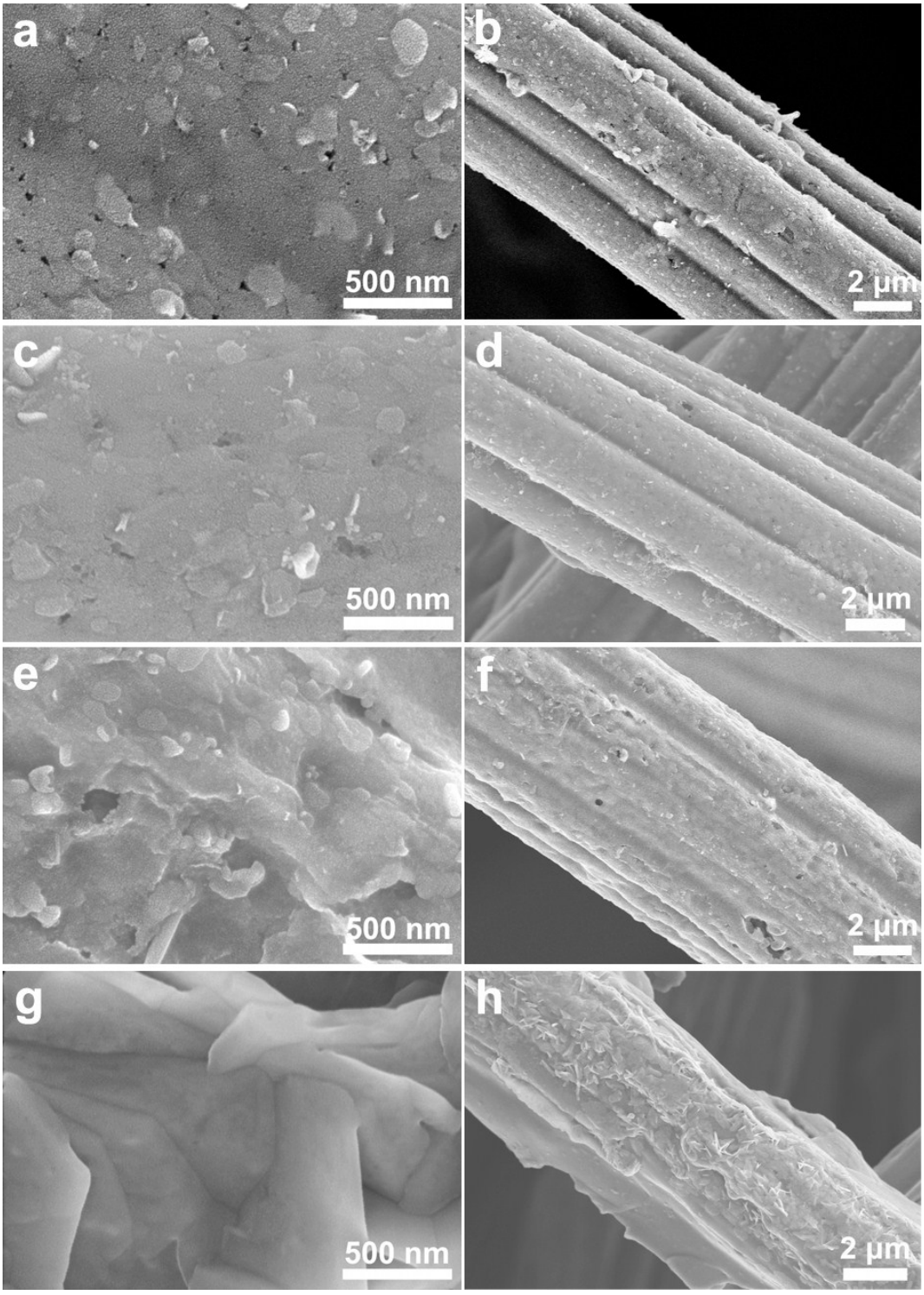

Fig. S16 The SEM images of CFC-450 after long term chronoamperometric measurement under different static potentials: (a, b) 1.375 V; (c, d) 1.454 V; (e, f) 1.725 V; (g, h) 1.935 V.

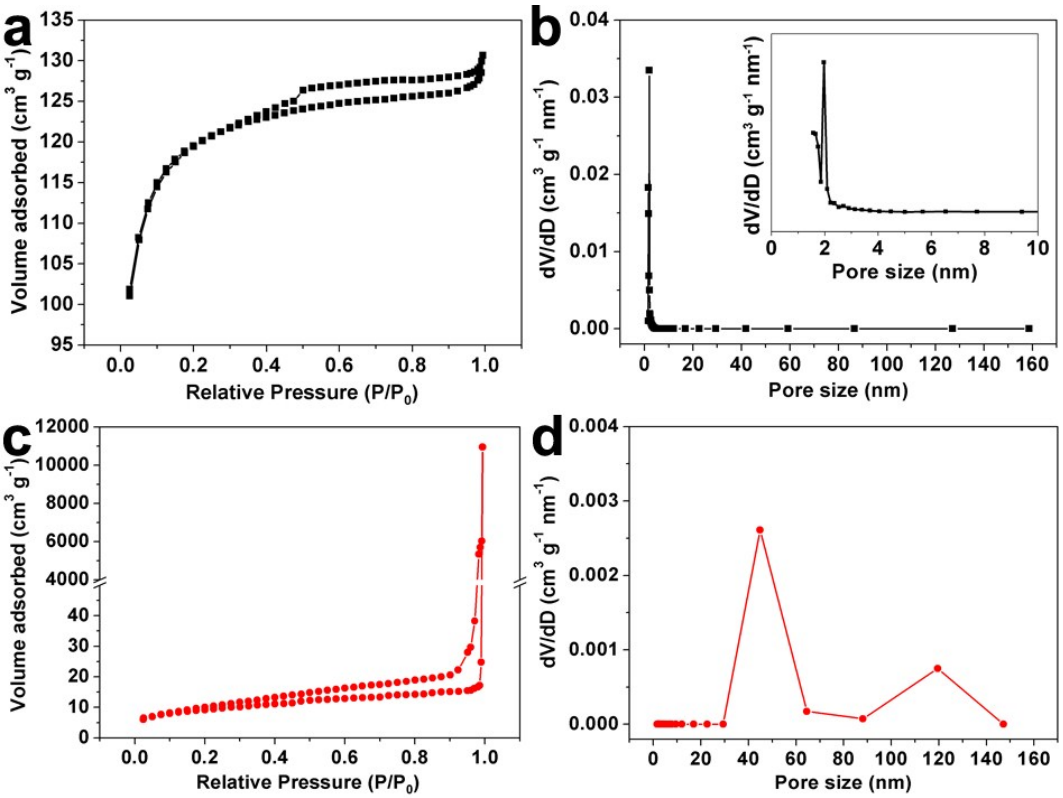

Fig. S17 Nitrogen sorption isotherms and pore size distributions of : (a, b) CFC-450 and (c, d) CFC-450 after long term chronoamperometric measurement under 1.375 V for 1 h, respectively.

Reference

1 M. Fujita, K. Wakabayashi, K. Nakada and K. Kusakabe, *J. Phys. Soc. Jpn.*, 1996, **65**, 1920-1923; K. Nakada, M. Fujita, G. Dresselhaus and M. S. Dresselhaus, *Phys.Rev.B*, 1996, **54**, 17954-17961; K. Wakabayashi, M. Fujita, H. Ajiki and M. Sigrist, *Phys.Rev.B*, 1999, **59**, 8271-8282; C. O. Girit, J. C. Meyer, R. Erni, M. D. Rossell, C. Kisielowski, L. Yang, C. H. Park, M. F. Crommie, M. L. Cohen, S. G. Louie and A. Zettl, *Science*, 2009, **323**, 1705-1708.

2 Z. Liu, Z. Zhao, Y. Wang, S. Dou, D. Yan, D. Liu, Z. Xia and S. Wang, *Adv. Mater.*, 2017, **29**,1606207-1606213.

3 Y. Zhang, X. Fan, J. Jian, D. Yu, Z. Zhang and L. Dai, *Energy Environ. Sci.*, 2017, **10**, 2312-2317.

4 X. Lu, W. L. Yim, B. H. Suryanto and C. Zhao, *J. Am. Chem. Soc.*, 2015, **137**, 2901-2907.

5 J. Lai, S. Li, F. Wu, M. Saqib, R. Luque and G. Xu, *Energy Environ. Sci.*, 2016, **9**, 1210-1214.

6 M. S. Balogun, W. Qiu, H. Yang, W. Fan, Y. Huang, P. Fang, G. Li, H. Ji and Y. Tong, *Energy Environ. Sci.*, 2016, **9**, 3411-3416.

7 Y. Jia, L. Zhang, A. Du, G. Gao, J. Chen, X. Yan, C. L. Brown and X. Yao, *Adv. Mater.*, 2016, **28**, 9532-9538.

8 Z. Xiao, X. Huang, L. Xu, D. Yan, J. Huo and S. Wang, *Chem. Commun.*, 2016, **52**, 13008-13011.

9 B. H. Suryanto and C. Zhao, *Chem. Commun.*, 2016, **52**, 6439-6442.

10 Y. Zhao, R. Nakamura, K. Kamiya, S. Nakanishi and K. Hashimoto, *Nat. Commun.*, 2013, **4**, 2390-2396.

11 C. Sheng, D. Jingjing, J. Mietek and Q. Shi Zhang, *Adv. Mater.*, 2014, **26**, 2925-2930.

12 T. Jingqi, L. Qian, A. A. M., A. K. A. and S. Xuping, *ChemSusChem*, 2014, **7**, 2125-2130.

13 T. Y. Ma, S. Dai, M. Jaroniec and S. Z. Qiao, *Angew. Chem., Int. Ed.*, 2014, **53**, 7281-7285.

14 N. Cheng, Q. Liu, J. Tian, Y. Xue, A. M. Asiri, H. Jiang, Y. He and X. Sun, *Chem. Commun.*, 2015, **51**, 1616-1619.

15 L. Qin, W. Yaobing, D. Liming and Y. Jiannian, *Adv. Mater.*, 2016, **28**, 3000-3006.

16 C. Tang, H. F. Wang, X. Chen, B. Q. Li, T. Z. Hou, B. Zhang, Q. Zhang, M. M. Titirici and F. Wei, *Adv Mater*, 2016, **28**, 6845-6851.

17 Q. Jiang, L. Xu, N. Chen, H. Zhang, L. Dai and S. Wang, *Angew. Chem., Int. Ed.*, 2016, **55**, 13849-13853.